

PACS numbers: 42.62.Fi; 78.47.jd; 78.67.Hc
DOI: 10.1070/QE2014v044n06ABEH015457

Effect of deuterium substitution for hydrogen in surface functionalisation of hydrophilic nanosilicon particles on their spectral and dynamic properties

V.O. Kompanets, S.V. Chekalin, S.G. Dorofeev, N.N. Kononov, P.Yu. Barzilovich, A.A. Ischenko

Abstract. **Broadband femtosecond spectroscopy has been used to study two types of hydrophilic silicon nanoparticles: (1) photoluminescent, passivated with deuterium and oxidised in fully deuterated dimethyl sulphoxide, and (2) nonluminescent (control samples having a similar crystalline core), passivated with hydrogen and oxidised in dimethyl sulphoxide. We have found significant differences in ultrafast spectral–temporal induced absorption dynamics between the two types of nanoparticles in the energy range corresponding to their calculated band gap. The observed distinction is due to the considerably higher oxidation rate of silicon on the surface of the deuterated samples in comparison with the undeuterated ones and with the associated increase in the number of photoluminescence centres on the surface of the nanoparticles. In the samples containing self-trapped exciton (STE) energy states responsible for the photoluminescence in the red spectral region, carrier capture at these levels and carrier relaxation to the ground state have characteristic times in the femtosecond range. In the samples free of STE states, excited carriers relax to the conduction band bottom in a characteristic time of several picoseconds.**

Keywords: *femtosecond spectroscopy, silicon quantum dots, charge carrier relaxation.*

1. Introduction

Because of the explosive growth in medical and biological applications of red fluorescent markers, the search for quantum dots (QDs) free of toxic ions has now become a critical issue. In connection with this, there is increased interest in crystalline nanosilicon-based QDs (Si-QDs). Silicon is known to be nontoxic and, moreover, it is one of the elements of life because it enters into the composition of a number of enzymes and proteins. The optical properties of Si-QDs are determined by both quantum confinement and silicon surface modification [1]. The red luminescence band of Si-QDs was interpreted in terms of an oxygen-related defect level, lying in the band gap of the silicon nanocrystals at nanoparticle diameters under 3 nm [2]. To date, many techniques for the synthesis of silicon nanoparticles with bright red and infrared luminescence have been proposed [3–5]. One of the most technologically feasible techniques among them is the chemical synthesis of Si-QDs from silicon monoxide [6–8], which was used in this study. Unfortunately, the photoluminescence quantum yield in Si-QDs is still rather low, which is mainly due to the nonradiative relaxation of excited carriers. A deep understanding of the processes responsible for the reduced luminescence efficiency is critical for the ability to improve the optical properties of silicon nanoparticles. Femtosecond absorption spectroscopy provides information about primary femto- and picosecond nonradiative relaxation channels for photoexcitation, and controlled engineering approaches enable targeted nanoparticle synthesis with the aim of verifying one mechanism or another.

In this paper, we report an experimental study of the influence of oxygen-related defect levels on the relaxation rate of excited carriers in Si-QDs. To this end, broadband femtosecond spectroscopy was used to gain insight into carrier excitation and relaxation processes in two types of hydrophilic Si-QDs having identical crystalline cores: (1) luminescent, passivated with deuterium and oxidised in fully deuterated dimethyl sulphoxide (DMSO-D6) and (2) nonluminescent, passivated with hydrogen and oxidised in dimethyl sulphoxide (DMSO).

2. Experimental

The nanocrystalline Si core used in the synthesis of the hydrophilic Si-QDs was prepared by the thermal annealing of silicon monoxide [6–8] at 400 °C. The average silicon core diameter in the nanoparticles was 2.5 ± 0.5 nm (as determined by small-angle X-ray scattering [8]). The core size was essentially independent of the SiO annealing temperature when it was within 900 °C. Hydrophilic nanosilicon sols were prepared by a process described elsewhere [7], with the following modifications: The SiO shell surrounding the Si core after annealing was etched by hydrofluoric acid-d (DF solution in D_2O) to give a deuterated material (D–Si-QDs) or by hydrofluoric acid (HF) to give a deuterium-free material (H–Si-QDs). To remove the acids, the nanoparticles were first washed with D_2O and H_2O, respectively. In the final washing and drying

V.O. Kompanets, S.V. Chekalin Institute of Spectroscopy, Russian Academy of Sciences, Fizicheskaya ul. 5, Troitsk, 142190 Moscow, Russia;
e-mail: kompanetsvo@isan.troitsk.ru, chekalin@isan.troitsk.ru;
S.G. Dorofeev Department of Chemistry, M.V. Lomonosov Moscow State University, Vorob'evy gory, 119991 Moscow, Russia;
e-mail: dorofeev_sg@mail.ru;
N.N. Kononov A.M. Prokhorov General Physics Institute, Russian Academy of Sciences, ul. Vavilova 38, 119991 Moscow, Russia;
e-mail: nnk@kapella.gpi.ru;
P.Yu. Barzilovich Institute of Problems of Chemical Physics, Russian Academy of Sciences, prosp. Akad. Semenova 1, 142432 Chernogolovka, Moscow region, Russia; e-mail: bpy@icp.ac.ru;
A.A. Ischenko Lomonosov Moscow State University of Fine Chemical Technologies, prosp. Vernadskogo 86, 119579 Moscow, Russia;
e-mail: aischenko@yasenevo.ru

Received 3 March 2014; revision received 20 March 2014
Kvantovaya Elektronika **44** (6) 552–555 (2014)
Translated by O.M. Tsarev

steps, solvents containing mobile hydrogen (methanol and acetone) were replaced by tetrahydrofuran purified by boiling over metallic sodium and then distilled. The nanoparticles separated by prolonged centrifugation were dissolved in DMSO-D6 and DMSO, respectively. In this process, the Si–D and Si–H surface groups were oxidized by dimethyl sulphoxide to Si–OD and Si–OH and the particles became hydrophilic. To prepare DF, we fabricated a four-compartment Teflon reactor, in which the acid was prepared by reacting sulphuric acid-d2 with an excess of dry fine calcium fluoride powder in flowing dry argon by a procedure described elsewhere [9].

Figure 1 shows linear absorption and luminescence spectra of the H–Si-QD and D–Si-QD samples. The absorption in the range 350–550 nm arises from the Si core and is the same in the two forms of nanosilicon. The band gap of the 2.5-nm nanoparticles, evaluated as described previously [8], is 2.4 eV. D–Si-QD luminescence was observed even during the second week after synthesis, whereas the H–Si-QDs showed negligible luminescence (Fig. 1). Note that, after passive oxidation with atmospheric oxygen, the photoluminescence of undeuterated nanosilicon sols in DMSO typically reaches its maximum level only after several months, whereas deuterated samples oxidize much more rapidly. It seems likely that this is primarily due to the lower D_3O^+ concentration in sols of deuterated samples in comparison with the H_3O^+ concentration in sols of undeuterated Si-QD samples, because the D_2O dissociation constant ($-\lg K_d = 14.7$, $T = 298$ K) is smaller than the H_2O dissociation constant ($-\lg K_d = 14.0$, $T = 298$ K). An increase in pH (pD) is known to be accompanied by a considerable increase in the oxidation rate of Si–D(H) groups on the surface of nanoparticles.

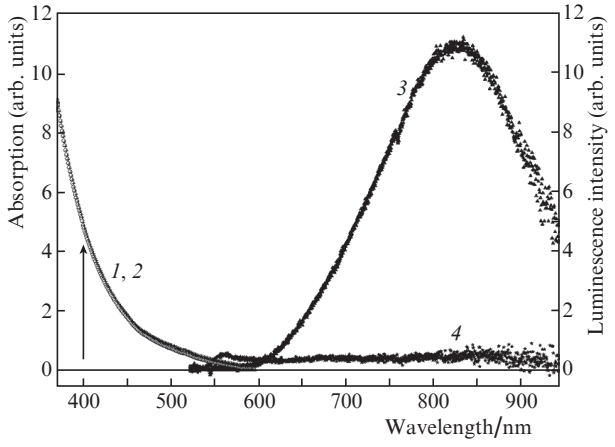

Figure 1. (*1*, *2*) Absorption and (*3*, *4*) luminescence spectra of (*1*, *3*) D–Si-QD deuterated and (*2*, *4*) H–Si-QD hydrogen-passivated nanosilicon sols obtained 11 days after synthesis. The arrow indicates the excitation wavelength in our experiments.

To assess photoinduced absorption changes, we used the pump–probe technique [10], with femtosecond pulses generated by a Ti:sapphire laser at a repetition rate of 1 kHz [11]. The laser output was divided by a beam splitter plate into two beams (excitation and probe), one of which was passed through an optical delay line. To excite the sample, the fundamental pulses were frequency-doubled (400 nm, ~100 fs). To probe the sample, the $\lambda = 800$ nm light was converted into a broadband supercontinuum pulse in a water-filled cuvette and then divided into two identical beams: a signal beam, I_s, which passed through the excitation zone in the sample, and a reference beam, I_r, which passed through the sample beyond the excitation zone. The two probe beams were focused into the sample and, after passing through it, were sent to a grating monochromator. Next, their spectra were measured using two linear diode arrays and, at each wavelength, the differential absorption signal was calculated as the negative logarithm of I_{s*}/I_s and I_{r*}/I_r ratios (where the asterisks refer to the signal measured under excitation). To obtain the signals under excitation and without it, the light was modulated at a frequency of 500 Hz by a chopper. In data processing, we took into account the dispersion-induced broadening of the broadband probe pulse (so-called chirp) and the contributions to the signal from a pure solvent (containing no nanoparticles) and the windows of the quartz cuvette.

The Si-QD sols were placed in the quartz cuvette (1 mm in thickness and ~1 cm^3 in volume), which was rotated to prevent degradation of the sample. At a photon energy of 3.1 eV, the excitation energy density was ~1 mJ cm^{-2}. The absorptance at the excitation wavelength was 50%, which corresponded to about one absorbed photon per nanoparticle at a nanoparticle concentration of 5×10^{15} cm^{-3}.

3. Experimental results and discussion

Figures 2a and 2b show the measured differential absorption spectra of our samples in the range 1.8–2.9 eV, and Figs 2c and 2d illustrate the induced absorption dynamics at three wavelengths after excitation by a 100-fs pulse at a photon energy of 3.1 eV. The observed difference in spectral dynamics is associated with the oxygen passivation of the silicon core and the presence of self-trapped exciton (STE) states, responsible for the efficient red luminescence [12], in the energy spectrum of the D–Si-QDs about 2.5 nm in size. After hydrogen passivation (in the H–Si-QDs), there are no such states, and the samples show no red luminescence. Luminescence is known to result from fast carrier capture at STE states during electron–phonon relaxation from excited states of the silicon core (which are referred to as free-electron levels in the literature) [13]. In our experiments, charge carriers were excited to rather high energy levels of the core and then relaxed from those levels to the conduction band bottom.

In the absence of oxygen-related defects capable of producing STE states, excited electrons relax to the conduction band bottom, where they reside for an indefinitely long time (on the timescale of our experiments, limited to 10^{-10} s). It is seen from the data in Figs 2a and 2b that, in the spectral region around 2.4 eV (band gap), the induced absorption in the H–Si-QDs relaxes to long-lived states with negative values. Given that the measured induced absorption is proportional to the difference between the excited-carrier absorption and the linear absorption in the sample, which is very weak at wavelengths above 600 nm (Fig. 1), we are led to conclude that, in this region, the excited-carrier absorption is weaker than the linear absorption. This fits well with the conclusion [13] that the free-carrier absorption is adequately described by the Drude theory, in which the absorption cross section is a quadratic function of wavelength [14]. Given that, in the case of quantum-size nanoparticles, the density of states increases with increasing carrier energy in the conduction band [15], it is reasonable to assume that, with increasing carrier energy, the free-carrier absorption will considerably increase with decreasing photon energy [13]. Based on these considerations,

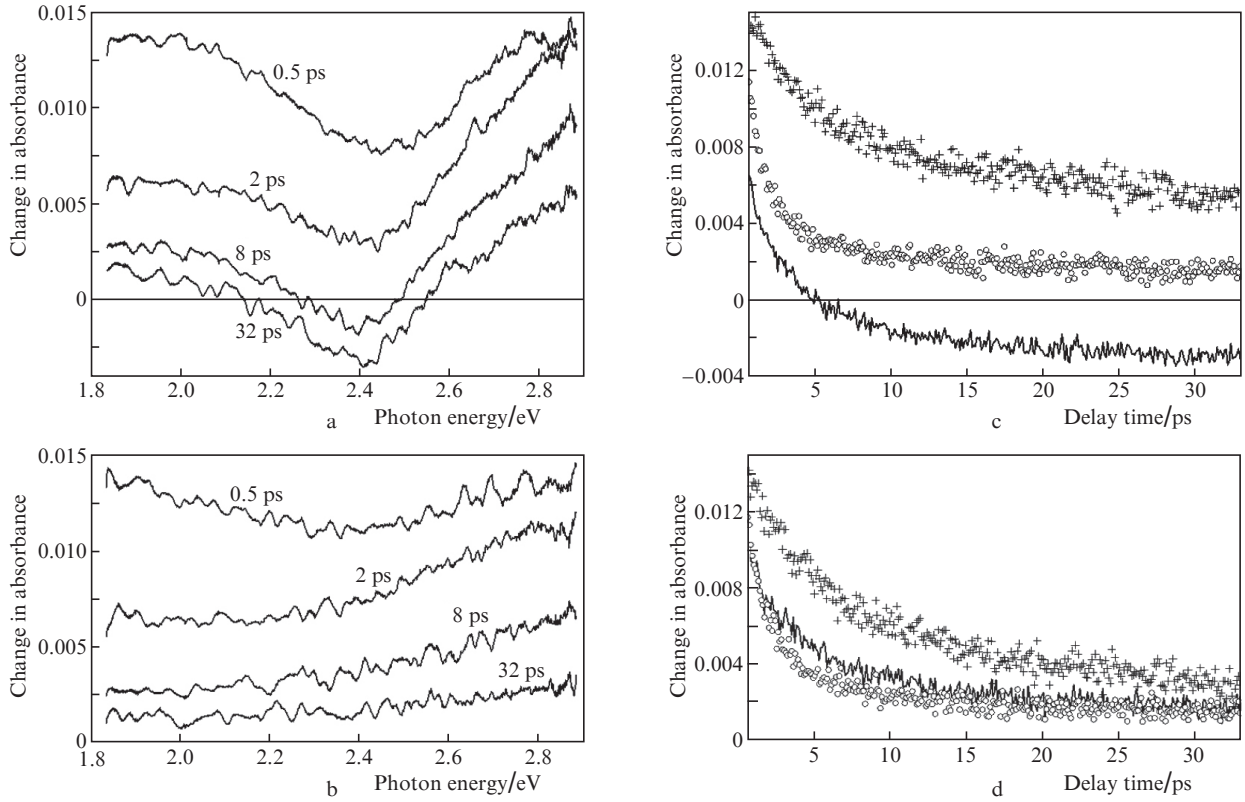

Figure 2. Induced absorption (a, b) spectra and (c, d) dynamics for (a, c) H–Si-QD hydrogen-passivated and (b, d) D–Si-QD deuterium-passivated nanosilicon sols under excitation at a photon energy of 3.1 eV. The delay times between the excitation and probe pulses are indicated in panels a and b. The absorption dynamics were probed at photon energies of 2.85 (crosses), 1.85 (circles) and 2.4 eV (solid lines).

we assign the induced free-carrier absorption in the IR spectral region primarily to high-energy excited states, whose relaxation to the conduction band bottom increases the fraction of the induced absorption in the visible range. In connection with this, we attribute the dynamics of spectral changes observed in the long-wavelength region in our pump–probe experiments to excited-carrier relaxation far from the conduction band bottom, whereas the changes in the shorter wavelength region reflect the behaviour of carriers near the band bottom.

It is worth pointing out that, in contrast to experiments reported by De Boer et al. [13], in which a significant role in the observed relaxation was played by Auger recombination and other effects associated with the high Si-QD concentration in the samples, the QD concentration in our experiments was three orders of magnitude lower, and the number of absorbed photons per Si-QD was no greater than unity. Because of this, we believe that the main free-carrier relaxation channel was electron–phonon relaxation. The fact that it could not be represented by a single exponential was due to the scatter in Si-QD size (this applies only to the Si-QDs containing no STE states). The induced absorption dynamics measured at different wavelengths (Figs 2c, 2d) demonstrate that this process is much faster far from the conduction band bottom (at a probe energy of 1.85 eV, the shortest time in fitting with three exponentials is 1 ps) than near the band bottom (at a probe energy of 2.85 eV, the shortest time is 5 ps).

Since the two types of samples had identical cores, they showed identical excitation and initial relaxation dynamics. This is evidenced by the fact that identical data were obtained in the long-wavelength region (induced 1.85-eV absorption dynamics in Fig. 2). In the samples free of STE states, complete electron–phonon relaxation of free carriers took place, bringing electrons to the conduction band bottom. The differential absorption spectrum then shows a bleach at wavelengths corresponding to the band gap (Fig. 2) because the excited-carrier absorption is weaker than the initial one. In the presence of defects, charge carriers can be rapidly captured at STE states in some stage of the relaxation process, without reaching the conduction band bottom, which shows up as a decrease in relaxation rate in such samples in the short-wavelength region in comparison with the nonluminescent samples (induced 2.85-eV absorption dynamics in Fig. 2). The characteristic capture rate in our experiments considerably exceeded the estimate reported by De Boer et al. [13]: 10^{10} to 10^{12} s^{-1}.

Since the relaxation dynamics of the induced 1.85-eV absorption are identical for the two samples without any fitting (Fig. 2), we are led to conclude that the number of excited carriers is also the same in the samples. Therefore, the difference between the induced absorption spectra of the luminescent and nonluminescent samples may provide additional information about details of carrier capture at self-trapped states. The results of such a procedure at several time delays are presented in Fig. 3. It is seen that, in the long-wavelength region, which, as mentioned above, characterises strongly excited charge carriers in the conduction band, the difference is nearly zero, lending further support to the conclusion that, far from the conduction band bottom, the charge carriers in the two samples are involved in identical processes. The absorption near 2.48 eV, observed even at a delay time of 0.5 ps, can be identified with the previously observed absorp-

tion from the bottom of a metastable defect state [16], determined by its optical ionisation energy.

We are thus led to conclude that, during this short time period, not only electrons were captured but they also relaxed to the STE band bottom. The shift of the absorption band in question to lower photon energies with increasing time delay (Fig. 3) can be accounted for by the filling of the STE band bottom with charge carriers. The origin of the negative signal at the short-wavelength edge is not yet clear, but it may be related to the subtraction of the free-electron absorption contribution near the conduction band bottom, which are missing in the samples with carriers captured at STE states.

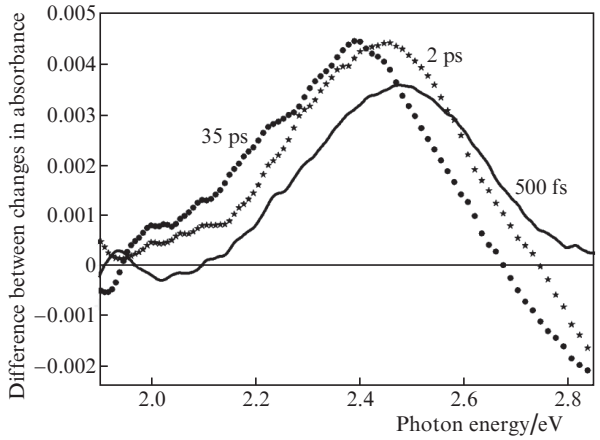

Figure 3. Differential induced absorption spectra of two types of nanoparticles at different delay times.

4. Conclusions

Investigation of ultrafast spectral–temporal induced absorption dynamics using broadband femtosecond probe pulses allowed us to track the excited-carrier relaxation dynamics in two types of silicon nanoparticles having identical crystalline cores 2.5 nm in size. We found significant differences in ultrafast spectral–temporal induced absorption dynamics between deuterated and undeuterated Si-QDs in the energy range corresponding to the calculated band gap of the nanoparticles. The observed distinction is due to the considerably higher oxidation rate of silicon on the surface of the deuterated samples in comparison with the undeuterated ones and with the associated increase in the number of photoluminescence centres on the surface of the nanoparticles.

In the samples containing STE energy states responsible for the luminescence in the red spectral region, carrier capture at these levels and carrier relaxation to the ground state have characteristic times in the femtosecond range. In the samples free of STE states, excited carriers relax to the conduction band bottom in a characteristic time of several picoseconds.

Acknowledgements. This work was supported in part by the Russian Foundation for Basic Research (Grant Nos 12-02-00840-a and 13-02-12407-OFI_m2) and the Presidium of the Russian Academy of Sciences (basic research programme 'Extreme Light Fields and Their Applications').

References

1. Dohnalova K., Poddubny A.N., Prokofiev A.A., de Boer W.D.A.M., Umesh C.P., Paulusse J.M.J., Zuilhof H., Gregorkiewicz T. *Light Sci. Appl.*, **2**, e47 (2013).
2. Wolkin M.V., Jorne J., Fauchet P.M., Allan G., Delerue C. *Phys. Rev. Lett.*, **82**, 197 (1999).
3. Canham L.T. *Appl. Phys. Lett.*, **57**, 1046 (1990).
4. Kumar V. (Ed.) *Nanosilicon* (Amsterdam: Elsevier, 2008).
5. Ischenko A.A., Fetisov G.V., Aslanov L.A. *Nanosilicon: Properties, Synthesis, Applications, Methods of Analysis and Control* (Boca Raton: CRC, 2014; Moscow: Fizmatlit, 2012).
6. Dorofeev S.G., Kononov N.N., Fetisov G.V., Ischenko A.A., Liaw D.J. *Nanotekhnika*, **3**, 3 (2010).
7. Dorofeev S.G., Kononov N.N., Ischenko A.A. *Nanotekhnika*, **1**, 62 (2012).
8. Dorofeev S.G., Ischenko A.A., Kononov N.N., Fetisov G.V. *Curr. Appl. Phys.*, **12**, 718 (2012).
9. Von Brauer G. (Ed.) *Handbuch der präparativen anorganischen Chemie* (Stuttgart: Ferdinand Enke, 1978; Moscow: Mir, 1985) Vol. 1.
10. Letokhov V.S. (Ed.) *Laser Picosecond Spectroscopy and Photochemistry of Biomolecules* (Bristol: Hilger, 1987; Moscow: Nauka, 1987).
11. Chekalin S.V. *Usp. Fiz. Nauk*, **176**, 657 (2006).
12. Allan G., Delerue C., Lannoo M. *Phys. Rev. Lett.*, **76**, 2961 (1996).
13. De Boer W.D.A.M., de Jong E.M.L.D., Timmerman D., Gregorkiewicz T., Zhang H., Buma W.J., Poddubny A.N., Prokofiev A.A., Yassievich I.N. *Phys. Rev. B*, **88**, 155304 (2013).
14. Smith R.A. *Semiconductors* (New York: Cambridge Univ. Press, 1959).
15. Gusev O.B., Poddubny A.N., Prokofiev A.A., Yassievich I.N. *Fiz. Tekh. Poluprovodn.*, **47** (2), 147 (2013).
16. De Boer W.D.A.M., Timmerman D., Gregorkiewicz T., Zhang H., Buma W.J., Poddubny A.N., Prokofiev A.A., Yassievich I.N. *Phys. Rev. B*, **85**, 161409(R) (2012).